

AEDC-TR-69-162

**ARCHIVE COPY  
DO NOT LOAN**

*copy!*



**SUPERSONIC COMBUSTION TESTS WITH A  
DOUBLE-OBLIQUE-SHOCK SCRAMJET  
IN A SHOCK TUNNEL**

**I. T. Osgerby, H. K. Smithson, and D. A. Wagner  
ARO, Inc.**

**PROPERTY OF U.S. AIR FORCE  
AEDC TECHNICAL LIBRARY**

**February 1970**

**TECHNICAL REPORTS  
FILE COPY**

This document has been approved for public release  
and sale; its distribution is unlimited.

**VON KÁRMÁN GAS DYNAMICS FACILITY  
ARNOLD ENGINEERING DEVELOPMENT CENTER  
AIR FORCE SYSTEMS COMMAND  
ARNOLD AIR FORCE STATION, TENNESSEE**

AEDC TECHNICAL LIBRARY



5 0720 00032 0226

PROPERTY OF U. S. AIR FORCE  
AEDC LIBRARY  
F40600 - 69 - C - 0001

# ***NOTICES***

When U. S. Government drawings specifications, or other data are used for any purpose other than a definitely related Government procurement operation, the Government thereby incurs no responsibility nor any obligation whatsoever, and the fact that the Government may have formulated, furnished, or in any way supplied the said drawings, specifications, or other data, is not to be regarded by implication or otherwise, or in any manner licensing the holder or any other person or corporation, or conveying any rights or permission to manufacture, use, or sell any patented invention that may in any way be related thereto.

Qualified users may obtain copies of this report from the Defense Documentation Center.

References to named commercial products in this report are not to be considered in any sense as an endorsement of the product by the United States Air Force or the Government.

SUPERSONIC COMBUSTION TESTS WITH A  
DOUBLE-OBLIQUE-SHOCK SCRAMJET  
IN A SHOCK TUNNEL

I. T. Osgerby, H. K. Smithson, and D. A. Wagner  
ARO, Inc.

This document has been approved for public release  
and sale; its distribution is unlimited.

## FOREWORD

The research reported herein was sponsored by Headquarters, Arnold Engineering Development Center (AEDC), under Program Element 62402F, Project 3012, Task 07.

The results of research reported herein were obtained by ARO, Inc. (a subsidiary of Sverdrup & Parcel and Associates, Inc.), contract operator of AEDC, Air Force Systems Command (AFSC), under Contract F40600-69-C-0001. The experimental tests were conducted under ARO Project No. VT5922, from June 1967 through December 1968, and the manuscript was submitted for publication on June 30, 1969.

This technical report has been reviewed and is approved.

Forrest B. Smith, Jr.  
Research Division  
Directorate of Plans  
and Technology

Harry L. Maynard  
Colonel, USAF  
Director of Plans  
and Technology

**ABSTRACT**

Some results of a continuing research program to develop a capability for testing integrated scramjets in the AEDC Tunnel F (Hotshot) are reported here. During this research program, an integrated double-oblique-shock scramjet model was developed to provide a test bed for supersonic combustion tests and for instrumentation development essential for analysis of combustion test results. Results are presented for tests in which hydrogen fuel was injected into the combustor. Injection of the fuel, from sonic orifices in the wall, normal to the flow did not lead to satisfactory combustion data, supposedly because of the cold boundary layer. Injection through sonic orifices in a series of diamond airfoil injectors led to combustion confirmed by all the following measurements (1) an increase in static pressure within the combustor downstream of the injection station, (2) an increase in surface heat-transfer rate, (3) an increase in static temperature as measured by the sodium line reversal technique, (4) an increase in output of radiation sensor gages, and (5) a decrease in flow Mach number inferred from static to pitot pressure measurements. The measured increases were proportionate to increases in computed average equivalence ratio. The combustion results are compared with numerical solutions. In general, the measured temperatures and pressures in the combustor with heat addition were higher than the calculated values.

## CONTENTS

	<u>Page</u>
ABSTRACT . . . . .	iii
NOMENCLATURE . . . . .	vii
I. INTRODUCTION . . . . .	1
II. TEST APPARATUS	
2.1 Tunnel and Test Conditions . . . . .	2
2.2 Model Configurations . . . . .	3
2.3 Instrumentation . . . . .	5
III. DEVELOPMENT OF THE MODEL FOR COMBUSTION TESTS	
3.1 Summary of Measurements on the Flat-Plate Inlet (Ramp) at 25 deg . . . . .	10
3.2 Summary of Measurements in the Combustor of the 25-deg Ramp Model . . . . .	11
3.3 Fuel Injection Tests with the 25-deg Ramp Model . . . . .	14
3.4 Summary of Measurements in the Combustor of the 27.5-deg Ramp Model . . . . .	14
IV. SUPERSONIC COMBUSTION TEST RESULTS	
4.1 Fuel Injection Tests with the 27.5-deg Ramp Model . . . . .	16
4.2 27.5-deg Ramp Model Tests with Heated Shock Tunnel Driver Gas Operation . . . . .	19
4.3 Fuel Injection Tests with the 27.5-deg Ramp Model and Heated Driver Gas Operation . . . . .	21
4.4 Sodium Line Reversal Temperature Measurements . . . . .	23
V. THEORETICAL COMBUSTION CALCULATIONS . . . . .	24
VI. CONCLUSIONS . . . . .	28
REFERENCES . . . . .	28

## ILLUSTRATIONS

<u>Figure</u>		
1.	Shock Tunnel I . . . . .	2
2.	Model with Foam Metal Ramp . . . . .	3
3.	Model Configurations, Instrumentation and Injection Modes . . . . .	4

<u>Figure</u>	<u>Page</u>
4. Strut Injector Detail . . . . .	5
5. Typical Pressure Traces . . . . .	6
6. Radiation Sensor Gage . . . . .	7
7. Relative Power Transmission of Water Vapor Bands versus Temperature . . . . .	8
8. Schematic of Sodium Line Reversal Equipment . . .	9
9. Static Pressures and Heat-Transfer Rates for Ramp at 25 deg . . . . .	10
10. Summary of Static Pressure Recovery . . . . .	12
11. Comparison of Solid and Porous Ramps on Combustor Performance (No Burning) . . . . .	13
12. Comparison of Combustor Pressures for 27.5- and 25-deg Ramp Angles . . . . .	16
13. Dimensionless Combustor Exit Pressures versus Equivalence Ratio (Cold Driver) . . . . .	17
14. Dimensionless Combustor Heat-Transfer Rates versus Equivalence Ratio (Cold Driver) . . . . .	18
15. Relative Output of Radiation Gages versus Equivalence Ratio (Cold Driver) . . . . .	19
16. Effect of Driver Gas Temperature and Ramp Density on Dimensionless Combustor Pressures (27.5-deg Ramp Model) . . . . .	20
17. Dimensionless Combustor Exit Pressures versus Equivalence Ratio (Hot Driver) . . . . .	21
18. Influence of Equivalence Ratio on Combustor Static Pressure Distribution . . . . .	22
19. Line Reversal Temperatures as a Function of Time .	23
20. Effect of Equivalence Ratio on Combustor Static Pressures and Temperatures for Constant Area Com- bustion (Nonequilibrium Theory) . . . . .	26
21. Effect of Equivalence Ratio on Combustor Static Tem- perature for Constant Pressure Combustion (Nonequi- librium Theory) . . . . .	27

## TABLES

	<u>Page</u>
I. Typical Test Conditions . . . . .	3
II. Model Design Conditions, Two-Shock Theory (Inviscid, 25-deg Ramp) . . . . .	15

## NOMENCLATURE

C	Conditions in the combustor behind the second oblique shock
$C_h$	Stanton number, $C_h \approx \dot{q}_w / \rho_\infty U_\infty (H_O - H_w \approx \dot{q}_w / \rho u (H_{adw} - H_w)$
$C^*$	Form of Chapman-Rubesin viscosity coefficient, $C^* = \mu^* T_\infty / \mu_\infty T^*$
ER	Equivalence ratio (fuel/air ratio)/(stoichiometric fuel/air rates)
H	Total enthalpy
$L_O$	Flame (or combustion) length
M	Mach number
P	Pressure
PM	Photomultiplier tube
Q	Denotes heat-transfer gage
$\dot{q}$	Heat-transfer rate, Btu/ft <sup>2</sup> -sec
R	Conditions on inclined flat-plate ramp
Re	Reynolds number
$R_\lambda^\circ$	Planck blackbody function evaluated at wavelength $\lambda$
T	Temperature, °K
t	Time
U	Velocity
$\bar{v}_\infty^*$	Hypersonic interaction parameter, $\bar{v}_\infty^* = M_\infty \sqrt{C^* / Re_\infty}$
X	Distance
$\alpha_\lambda$	Integrated intensity of a water vapor band centered at wavelength $\lambda$

$\lambda$	Wavelength
$\mu$	Viscosity
$\rho$	Density
$\tau_{ID}$	Ignition delay
$\tau_R$	Reaction (or heat release) period
$\infty$	Free stream

**SUBSCRIPTS**

adw	Conditions evaluated at adiabatic wall temperature
C	Conditions in the combustor behind the second oblique shock
ex	Conditions at the exit plane of the combustor
i	Initial
o	Reservoir (total)
R	Conditions on the ramp inlet behind the first oblique shock
SLR	Sodium line reversal measurement
w	Conditions evaluated at the wall temperature (300°K)
$\infty$	Free-stream condition in tunnel test section

**SUPERSCRIPTS**

'	Stagnation condition (pitot)
*	Conditions evaluated at reference temperature

## SECTION I INTRODUCTION

A program is underway to evaluate the feasibility of using the 100-in. hypervelocity tunnel (Gas Dynamic Wind Tunnel, Hypersonic (F)) of the von Karman Gas Dynamics Facility (VKF) (Refs. 1 and 2) for testing integrated scramjet models. Tunnel F is an arc-heated hypervelocity (hotshot) wind tunnel with 108-in.-diam test section (Mach numbers from 14 to 22) and a 54-in. test section (Mach numbers from 10 to 18). A useful run time of between 50 and 200 msec is attained. In terms of Mach number and Reynolds number, a wide range of flight conditions is simulated, using nitrogen as the test gas. The results of a series of tests using air as a test gas were reported in Ref. 3. It was demonstrated that clean (unvitiated) airflow could be generated at a stagnation temperature of 3000°K and reservoir pressures up to 10,000 psia. Current tunnel development programs (including an enlarged arc chamber) are aimed at increasing this capability to 4000°K stagnation temperature at 20,000-psia pressure, or 2000°K at 40,000 psia.

A concurrent program was initiated to develop the instrumentation and theoretical tools necessary to obtain and analyze data during a test of a scramjet model in the tunnel. Such a program required a model with which the above development could be carried out. The results reported here were obtained in this development program.

A test program was initiated with an inclined flat-plate model similar to the program reported in Refs. 4 and 5, in which hydrogen fuel was injected upstream of an inclined plate into a Mach number 3 free stream (vitiated to raise the total enthalpy). The resulting fuel/air mixture passed through an oblique shock generated by an inclined plate at an angle of  $\approx 28$  deg. However, when this test configuration was set up in the hypersonic tunnels, the shock waves and wake generated by the injector assembly considerably modified the distribution of static pressure and heat-transfer rate on the surface of the inclined plate, even without fuel injection (Ref. 6). Hence the static temperature distribution behind the oblique shock would be an unknown and very nonuniform quantity. To overcome these obvious deficiencies, a double-oblique-shock model was developed (Ref. 6) so that fuel could be injected into a supersonic (as opposed to hypersonic) stream in the model combustor behind the second shock. The development of this model entailed a good deal of experimental research; thus the test program was conducted in the AEDC-VKF 16-in. Counterflow Range I (Refs. 7 and 8). The development of the model and results of aerodynamic and combustion performance tests in Tunnel I are presented.

## SECTION II TEST APPARATUS

### 2.1 TUNNEL AND TEST CONDITIONS

Tunnel I is a shock tunnel with a 16-in.-diam test section. A photograph of the tunnel is presented in Fig. 1. Helium at pressures up to 13,000 psia and at temperatures of 300 or 480°K is used as the driver gas. A double diaphragm separates the driver and driven tube sections. The gas pressures in the driver and driven tube can be accurately controlled before venting the gas between the diaphragms to initiate the run.

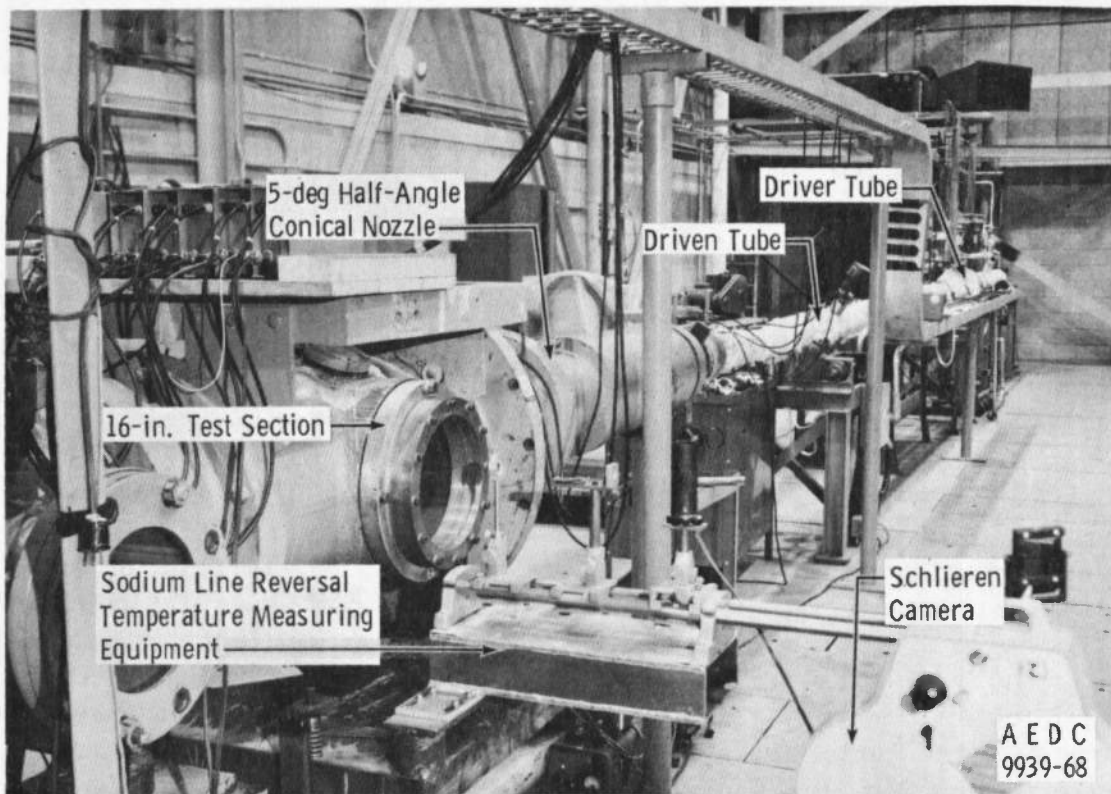


Fig. 1 Shock Tunnel I

The shock tunnel is operated in the tailored-interface mode. The shock heated air is expanded through a 5-deg half-angle conical nozzle to a free-stream Mach number  $\approx 11$  at the 16-in.-diam test section. Nominal test section conditions are presented in Table I.

TABLE I  
TYPICAL TEST CONDITIONS

Driver Gas Temperature, °K	$M_\infty$	$Re_\infty$ /ft	$P_{O_2}$ , psia	$T_{O_2}$ , °K	$P'_{O_2}$ , psia	$T_\infty$ , °K	$P_\infty$ , psia
300	11	$3.38 \times 10^6$	10,000	1860	18.0	88	0.120
480	10.9	$2.22 \times 10^6$	11,300	2270	19.2	110	0.127

## 2.2 MODEL CONFIGURATIONS

A photograph of the model with diamond airfoil (strut) injectors and with the flat plate (ramp) inclined at an angle of 25 deg is presented in Fig. 2. Details of model geometry, fuel injection mode (fuel is injected from a plenum chamber in the top combustor plate), and instrumentation layout are shown in Fig. 3.

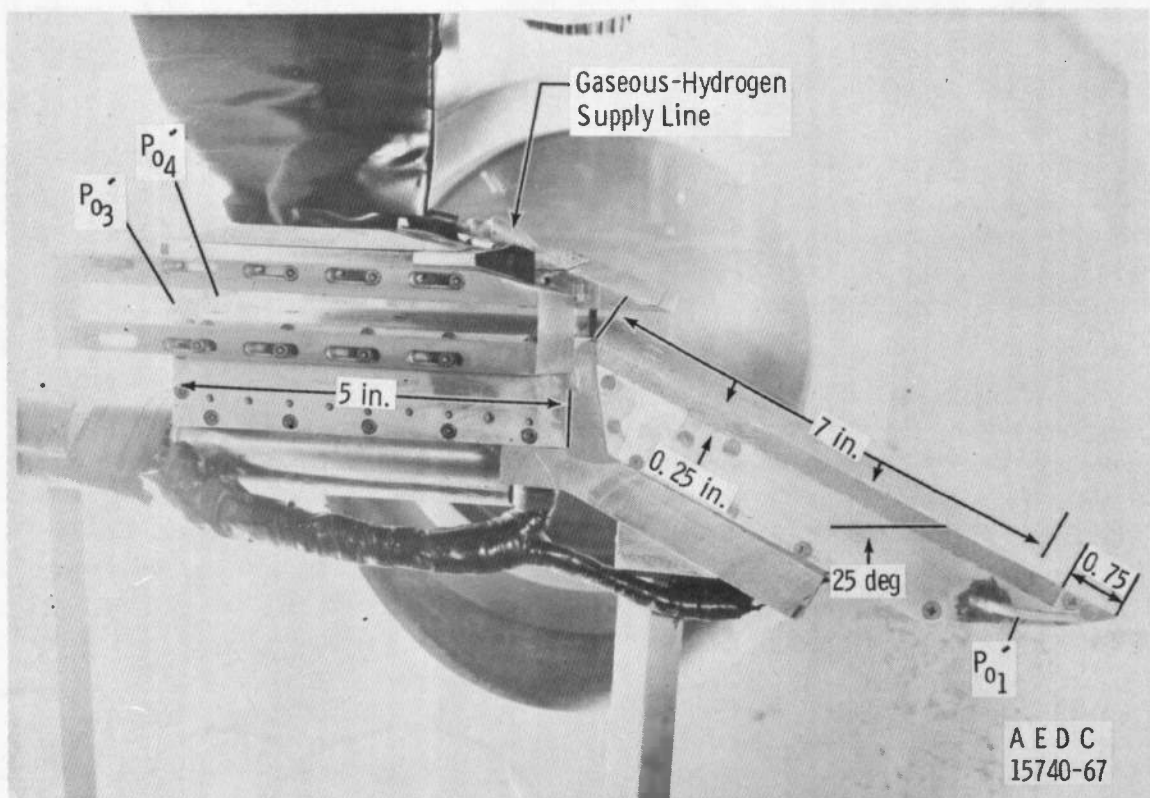


Fig. 2 Model with Foam Metal Ramp

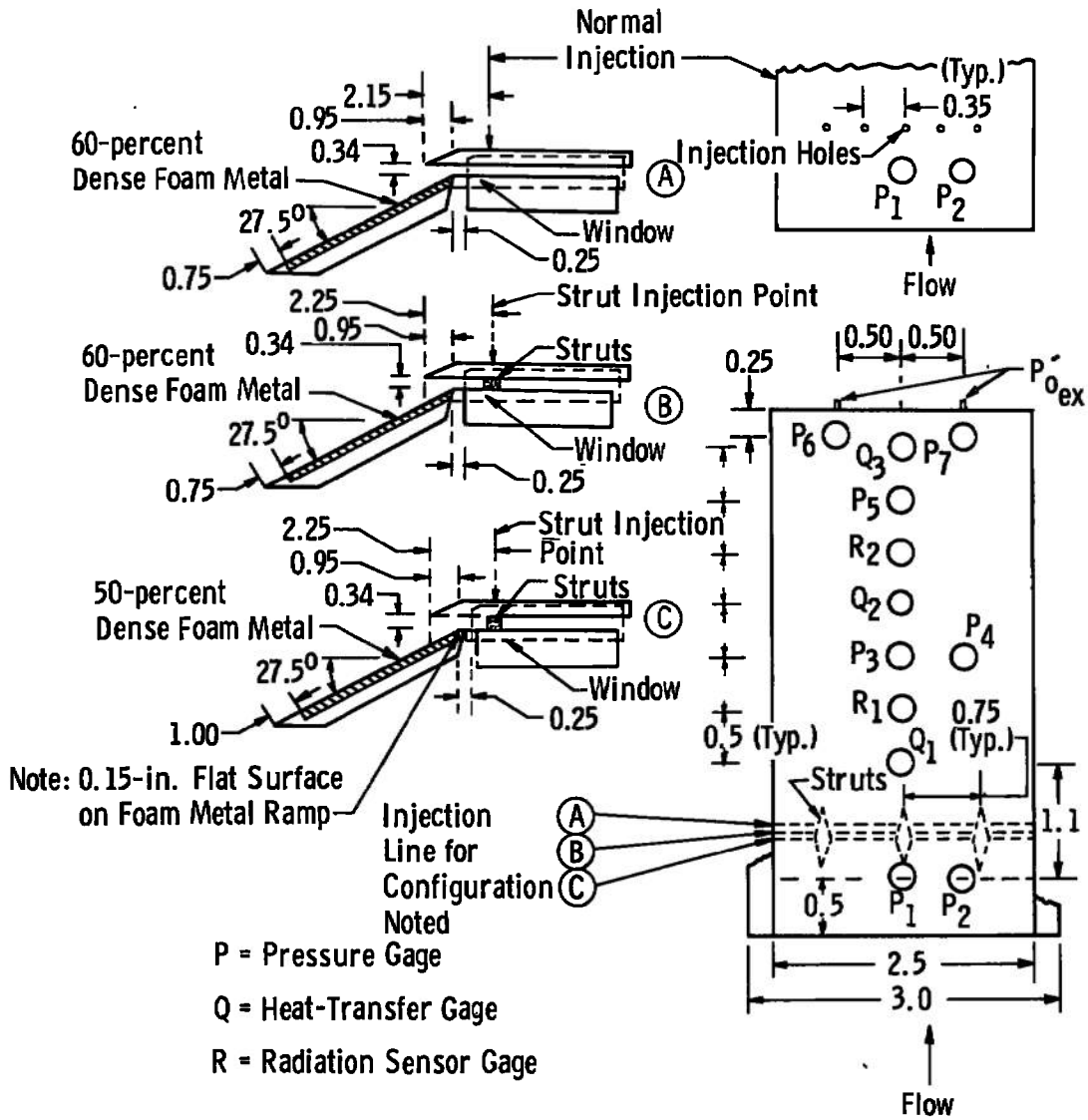


Fig. 3 Model Configurations, Instrumentation and Injection Modes

Normal injection was accomplished by means of five 0.032-in.-diam sonic orifices spaced 0.35 in. apart and symmetrically located about the axial centerline of the model. For the strut injection system, the struts were placed 0.75 in. apart and symmetrically about the axial centerline of the model. Details of the strut injectors are shown in Fig. 4.

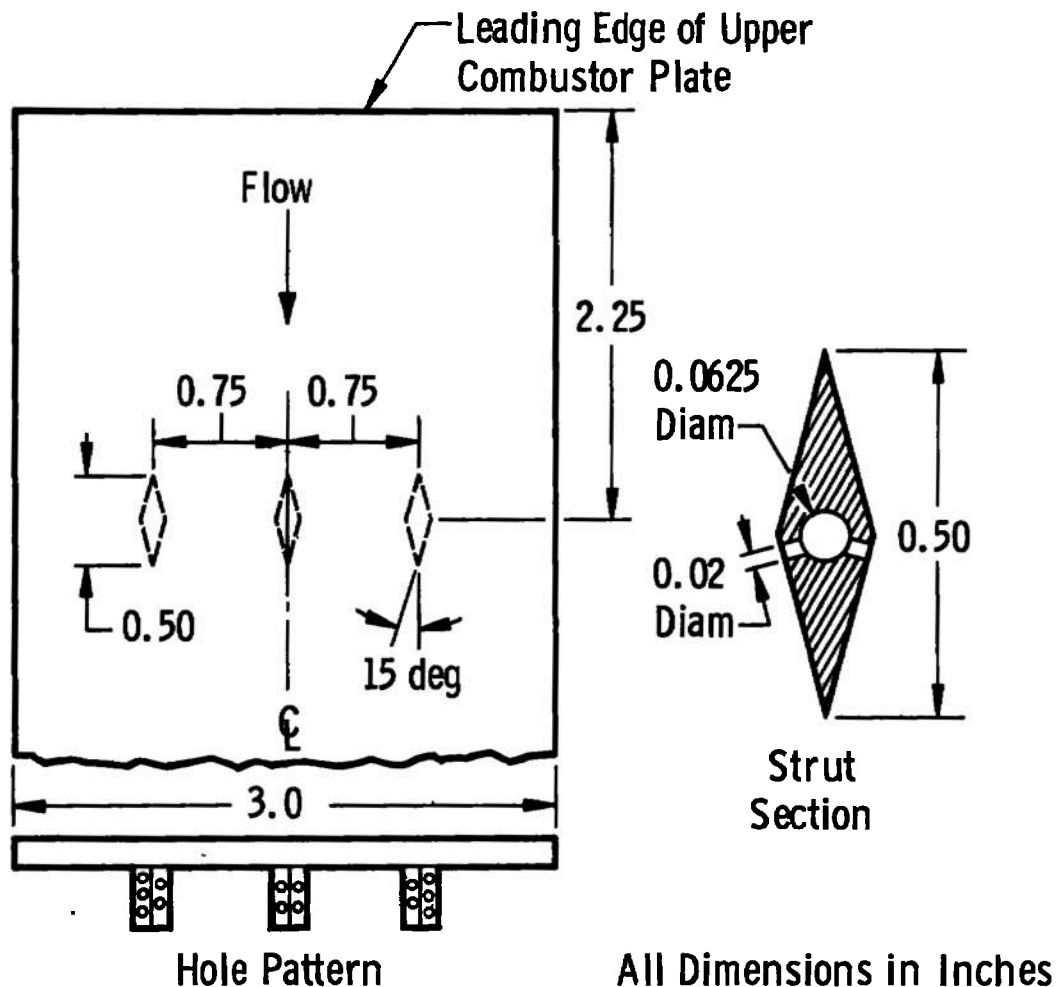


Fig. 4 Strut Injector Detail

## 2.3 INSTRUMENTATION

### 2.3.1 Pressures

Piezoelectric pressure transducers were used to measure the total pressure in the reflected shock region and the free stream and model pitot pressures. Diaphragm-type pressure transducers were used to measure surface pressures in the model.

Typical reservoir pressure, test section pitot pressure, and model combustor exit pitot pressure traces are shown in Fig. 5. Test data were taken during the period of constant pitot pressure. The start time of the tunnel was approximately 1 msec, and the start time of the model was negligible, as shown. The useful test time was approximately 3 msec.

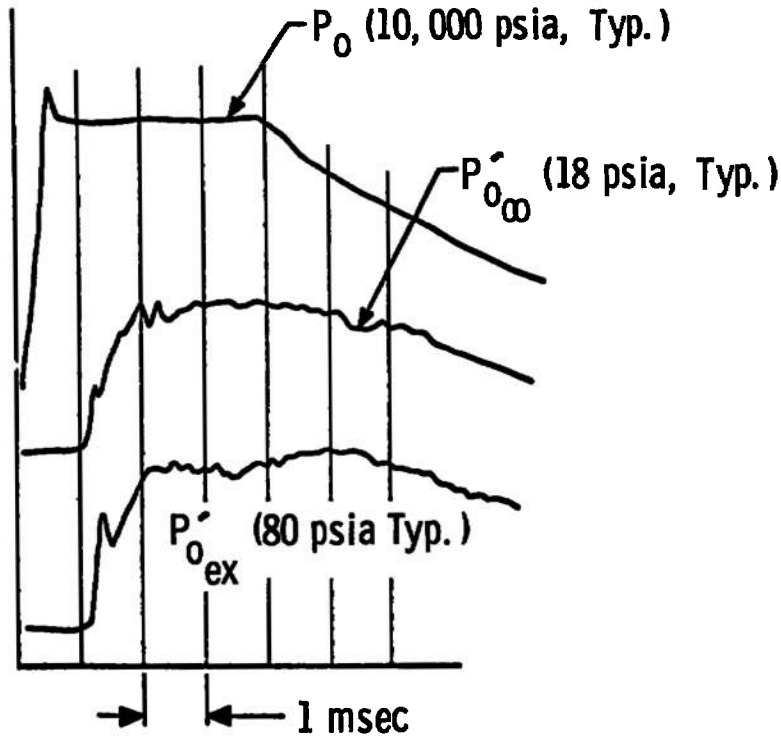


Fig. 5 Typical Pressure Traces

### 2.3.2 Shock Velocity

Thin-film shock-velocity detectors were placed at intervals along the shock tube. In addition to velocity measurement, these gages were used to trigger electronic recording equipment.

### 2.3.3 Heat-Transfer Rates

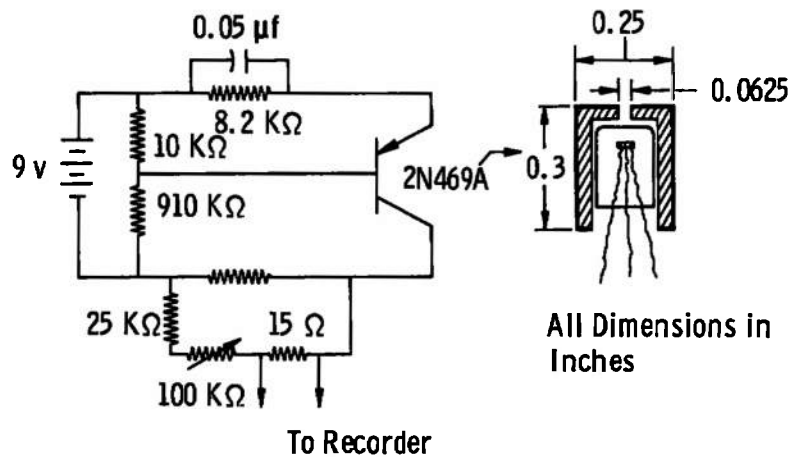
The model surface heat-transfer gages were 0.020-in.-thick slug calorimeters with a thin-film resistance temperature sensor. Additional information on these gages and the pressure transducers is given in Ref. 9.

### 2.3.4 Flow Visualization

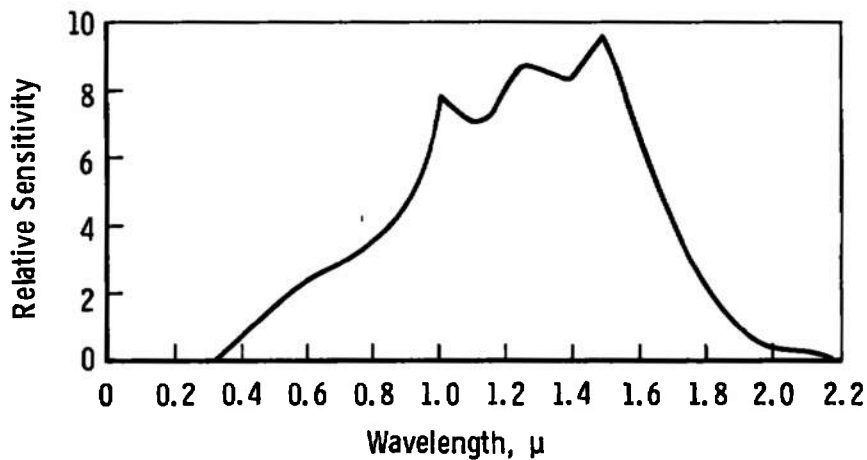
Schlieren motion pictures were obtained at 5000 frames per second by means of a Hi-Cam® camera. Both color and black and white schlieren pictures were obtained.

### 2.3.5 Radiation Sensors

Phototransistors were used as a qualitative method of detecting hydrogen burning. A sketch of the phototransistor and circuitry is shown in Fig. 6a. The relative sensitivity of the radiation gage as a function of wavelength is shown in Fig. 6b.



a. Radiation Gage Schematic



b. Relative Sensitivity of Radiation Gage

Fig. 6 Radiation Sensor Gage

The wavelength cutoff of the radiation gage is in the near infrared, whereas the strongest radiation bands for water vapor occur beyond the cutoff point. The relative power radiated by the different water vapor bands can be estimated from the product of the ratios of the relative integrated intensity ratios ( $\alpha_\lambda$ ) evaluated at the band centers and the ratios of the Planck blackbody functions ( $R_\lambda^0$ ) evaluated at the band centers at wavelength  $\lambda$ . The results of this simplified calculation are presented in Fig. 7, using integrated intensity data from Ref. 10. Radiation from band centers at 1.1, 1.38, and 1.8  $\mu$  are transmitted. The bandpass of the phototransistor is seen to encompass a significant portion of the radiation from the water vapor bands.

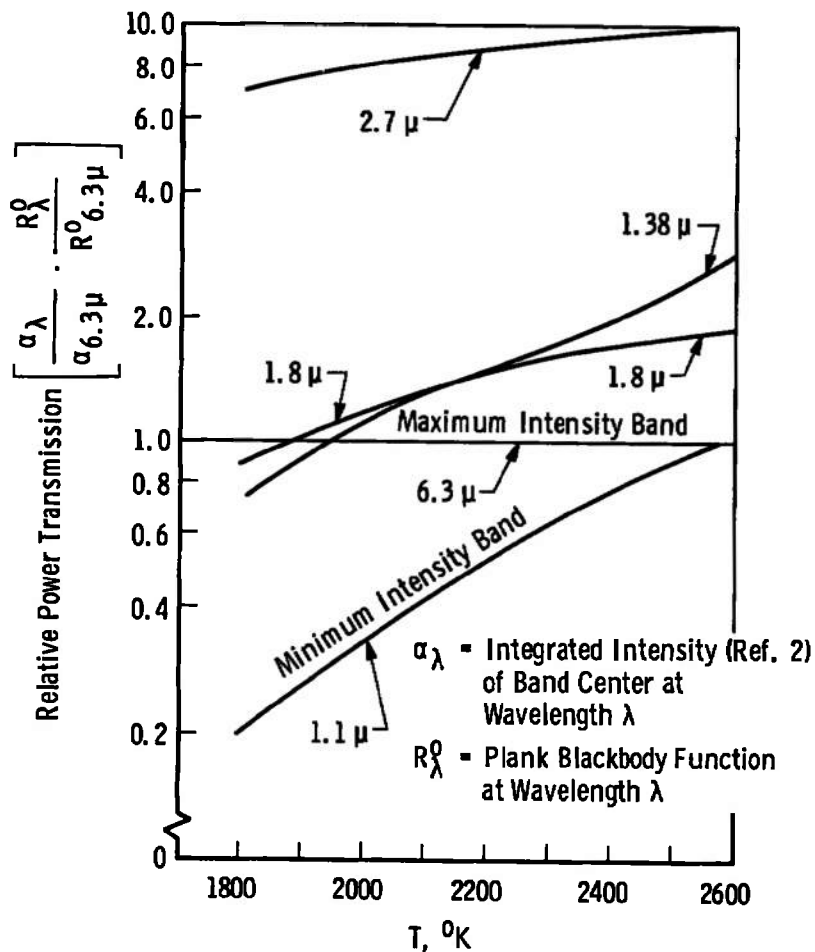


Fig. 7 Relative Power Transmission of Water Vapor Bands versus Temperature

### 2.3.6 Sodium Line Reversal Temperature Measurements

Static temperatures in the combustor were determined by the sodium line reversal method using a single-beam technique similar to that described in Ref. 11. A schematic of the line reversal equipment installed on its vibration isolation unit is shown in Fig. 8. The image of the tungsten filament lamp is focused on the axial centerline of the combustor. The knife edge is adjusted so that one of the phototubes (PM1) sees only the emission from the hot gas (seeded with sodium chloride), and the other phototube (PM2) sees the lamp filament image through the hot gas. The ratio of the output of PM1 to the difference in outputs of PM1 and PM2 is equal to the ratio of the Planck blackbody functions evaluated at the gas temperature and the brightness temperature of the lamp filament at the reversal wavelength. The aperture and field stop shown in Fig. 8 are used to equalize the solid angles, illuminated area, and response of the two phototubes so that respective slit functions, etc., for each phototube can be eliminated from the temperature calculation.

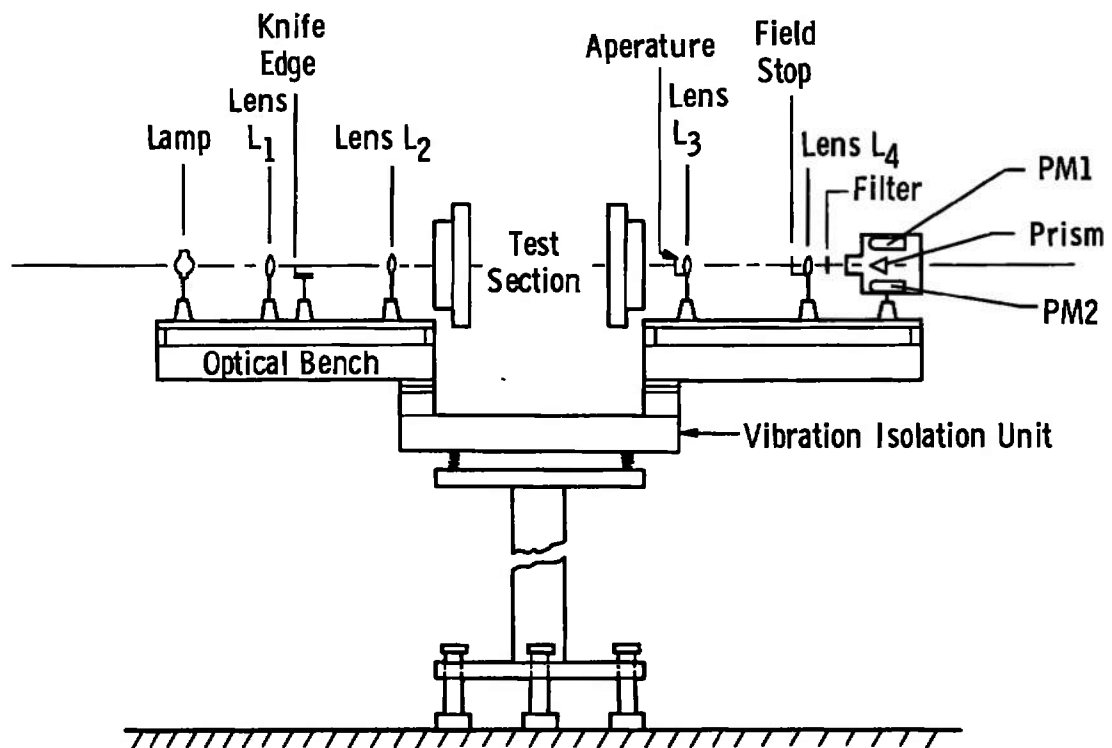


Fig. 8 Schematic of Sodium Line Reversal Equipment

**SECTION III  
DEVELOPMENT OF THE MODEL FOR COMBUSTION TESTS**

The object of the model development tests was to produce static pressures and temperatures at a supersonic Mach number in the model combustor which would support spontaneous combustion of hydrogen fuel injected into the flow. Calculations were made assuming inviscid, adiabatic, two-shock operation, and it was determined (Ref. 6) that flow deflection angles of 25 deg should be more than adequate (allowing a safe margin for mixing of the hydrogen/air). Accordingly, such a double-oblique-shock model was fabricated, and a series of aerodynamic tests was initiated. Detailed results were documented in Ref. 6.

**3.1 SUMMARY OF MEASUREMENTS ON THE FLAT-PLATE INLET (RAMP) AT 25 DEG**

Summary plots of the measured static pressures and heat-transfer rates are shown in Fig. 9. The decay in static pressure along the plate surface is caused by source flow effects in the 5-deg half-angle nozzle, as shown in Ref. 6. The experimental heat-transfer rates indicate that the end of transition from a laminar to a turbulent boundary layer occurred at approximately 3 in. from the plate leading edge, whereas the estimated length for the end of transition (using current transition literature) was approximately 6 to 7 in.

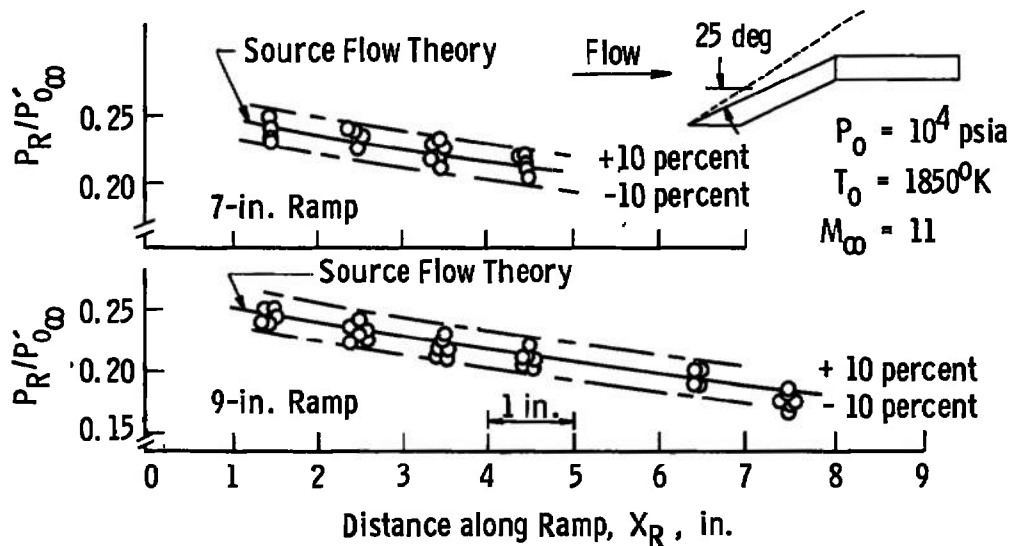
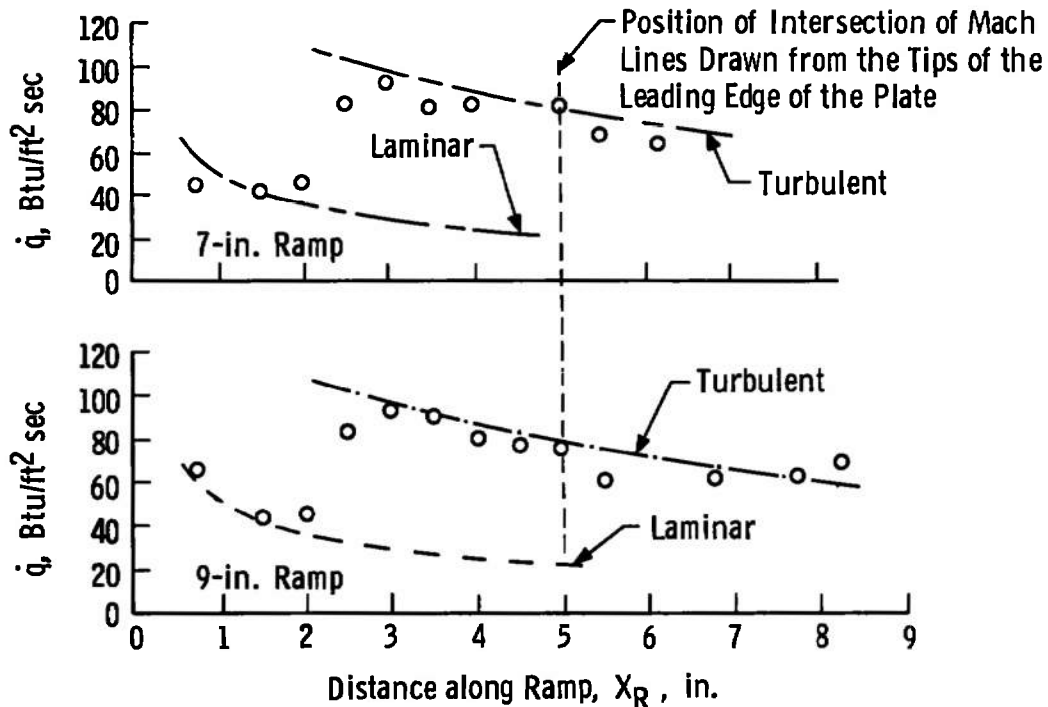


**Fig. 9 Static Pressures and Heat-Transfer Rates for Ramp at 25 deg**



b. Heat Transfer  
Fig. 9 Concluded

### 3.2 SUMMARY OF MEASUREMENTS IN THE COMBUSTOR OF THE 25-DEG RAMP MODEL

Summary plots of the ratio of measured static pressures in the combustor referenced to the free-stream stagnation pressure are shown in Fig. 10. Tests were conducted without sidewalls on the combustor, and a considerable decay in static pressure was observed. The smooth decay suggests that expansion waves generated by edge effects caused the decay resulting in outflow and hence significant mass flow losses from the open sides. Sidewalls were installed on the model to prevent this outflow of air from the combustor; however, the pressure ratio at the entrance to the combustor was reduced from 1.17 for the open sidewall tests to 0.8. Evidently, losses of considerable magnitude were introduced by the installation of sidewalls. It was established in Ref. 6 that these losses were caused by the inlet boundary layer modifying the interaction of the shock from the cowl lip with the Prandtl-Meyer expansion fan at the junction of the inlet and combustor and the additional interference of the shock waves from the combustor sidewalls. Schlieren motion pictures indicated that the boundary layer on the flat-plate inlet (ramp) was separated at the combustor entrance, effectively increasing the contraction ratio. On several tests, the model did not start resulting in

unsteady, choked flow in the combustor. A porous plate inlet was substituted for the solid plate in order to bleed off the low momentum portion of the boundary layer and reduce the pressure losses caused by separation phenomena. The resulting pressure distribution was significantly improved, as shown in Fig. 10; however, no additional improvement in pressure ratio was obtained. Pitot pressures (measured at the combustor exit plane) referenced to the reservoir total pressure, together with estimated combustor exit Mach numbers, are shown in Fig. 11. In general, the higher pitot pressures were obtained with the second shock impinging as closely as possible to the junction between the flat-plate inlet (ramp) and combustor. This condition apparently gives the most effective cancellation of the expansion fan by the cowl-lip shock.

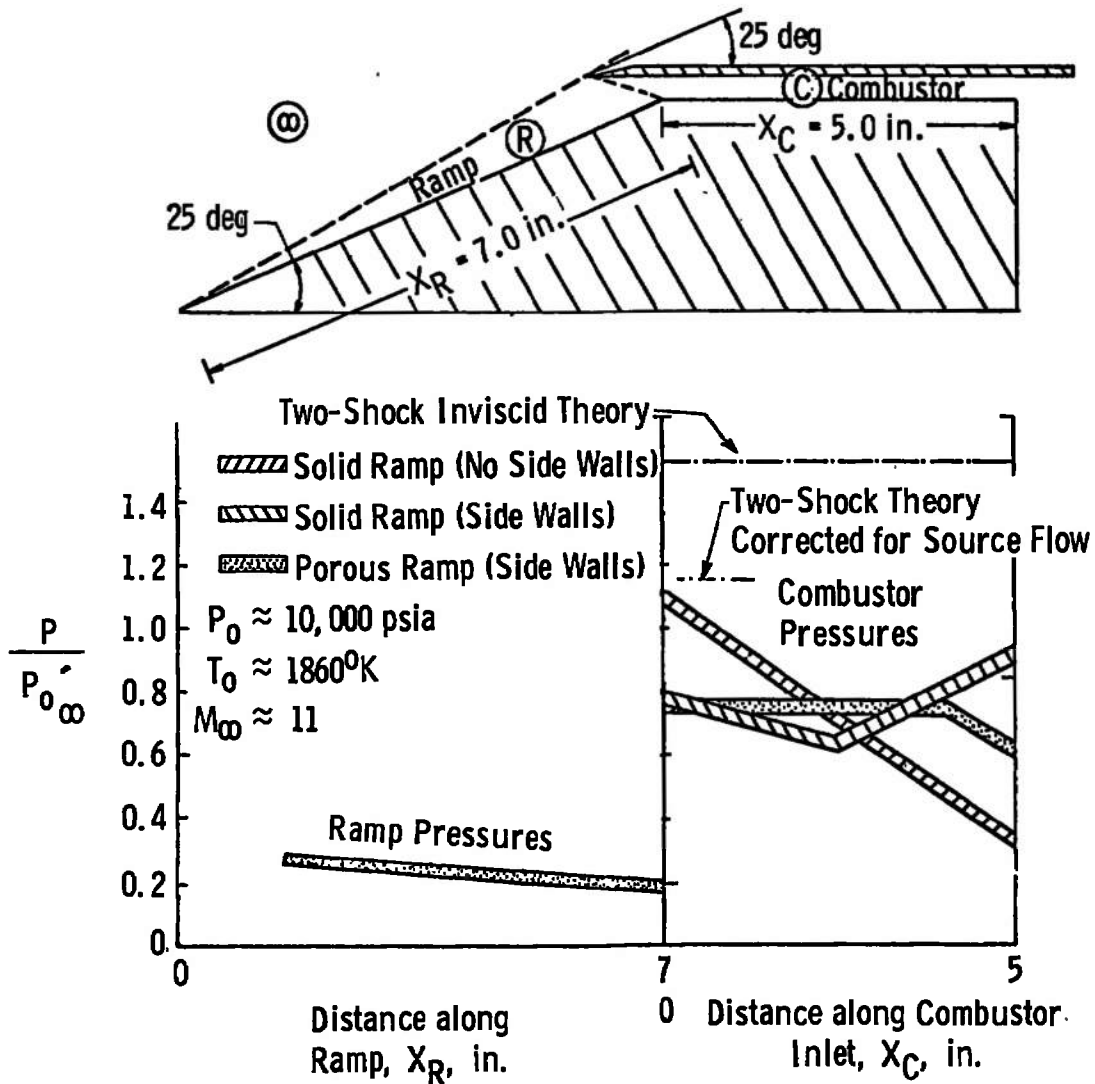


Fig. 10 Summary of Static Pressure Recovery

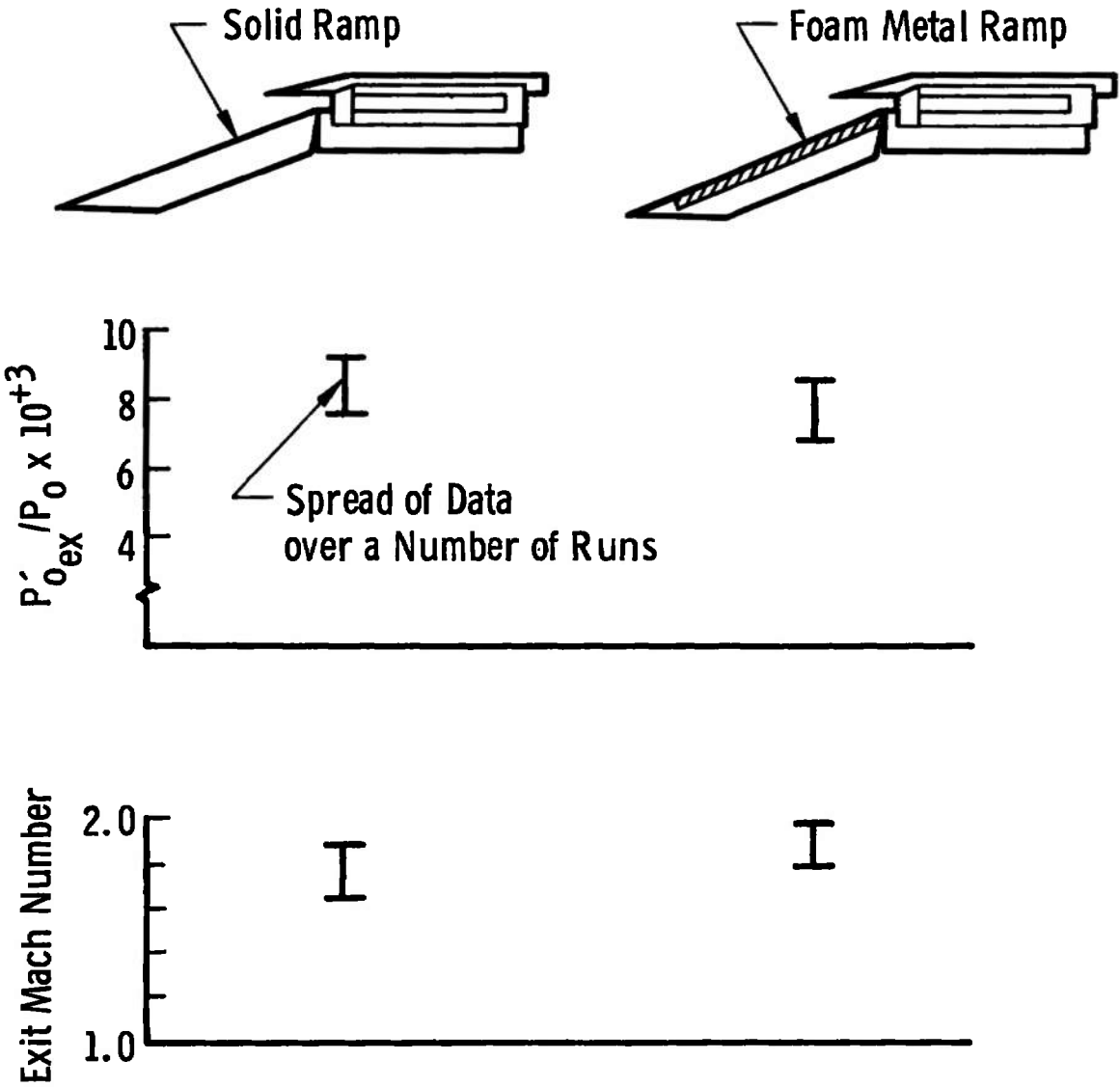


Fig. 11 Comparison of Solid and Porous Ramps on Combustor Performance (No Burning)

### 3.3 FUEL INJECTION TESTS WITH THE 25-DEG RAMP MODEL

Hydrogen fuel, at 300°K total temperature, was injected from a row of sonic orifices in the upper surface of the combustor (see Fig. 3). This injection mode was designated normal injection. No combustion was observed for a wide range of equivalence ratios. Without fuel injection, the average static pressure in the combustor was  $\approx 0.92$  atm, the estimated static temperature of the air was  $\approx 1200^\circ\text{K}$ , and the combustor flow Mach number was  $\approx 1.9$ .

The experimentally measured combustor pressures with no fuel injected were approximately 50 percent below the inviscid two-shock theory value, and although a small static temperature increase above the theory value was estimated, the estimated combustion time was approximately doubled. Estimates were based on the results of Ref. 12. When an additional allowance was included to account for the cooling effect of injecting the hydrogen at a total temperature of 300°K, the calculated overall combustion time was approximately three times the value shown in Table II. Assuming the combustor flow velocity remained essentially constant, the combustor length required for complete combustion would be 4.5 in. (i. e., 0.5 in. more than the available model combustor length) even without including a finite length for mixing delay. The static temperature necessary to compensate for the considerable pressure losses and the injectant cooling is 1520°K. Calculations indicated that an increase in total enthalpy obtained with an increase in the shock tunnel driver gas (helium) temperature from 300 to 480°K, should provide the necessary compensation for the above performance deficiencies.

### 3.4 SUMMARY OF MEASUREMENTS IN THE COMBUSTOR OF THE 27.5-DEG RAMP MODEL

The flow deflection angles were increased to 27.5 deg to generate a higher static pressure and temperature in the combustor. It was hoped that the higher static pressure on the ramp would force more of the ramp boundary layer through the porous metal, resulting in lower total pressure losses caused by reduced separation phenomena at the intersection of the ramp and combustor. The measured pressures are shown in Fig. 12. Apart from a small improvement in pressure distribution, no significant increase in pressure level occurred. Possibly the increase in inclination of the ramp produced sufficiently higher edge losses to compensate for the increase in shock pressure ratio. (The porous ramp was not instrumented.)

**TABLE II**  
**MODEL DESIGN CONDITIONS, TWO-SHOCK THEORY (INVISCID, 25-DEG RAMP)**

Station	$\omega$	R	C
P, psia	0.12	4.8	27.3
T, °K	88	647	1160
M	11.0	3.5	2.1
U, ft/sec	6789	5819	4635
$\tau_{ID}$ , $\mu$ sec	--	--	17
$\tau_R$ , $\mu$ sec	--	--	10
$L_0$ , in. ...	--	--	1.50

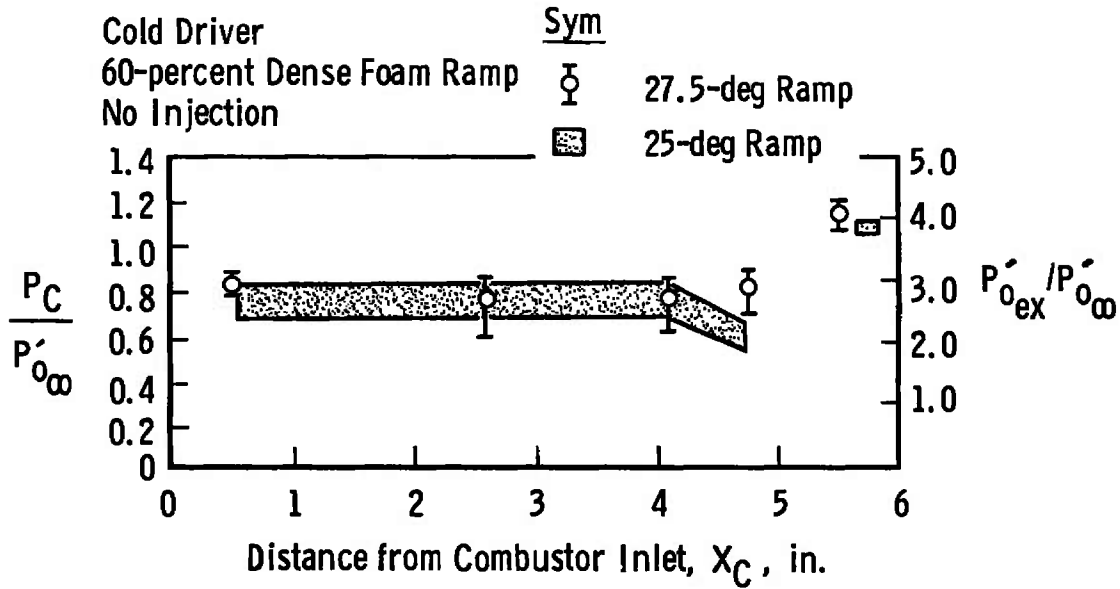


Fig. 12 Comparison of Combustor Pressures for 27.5- and 25-deg Ramp Angles

**SECTION IV**  
**SUPERSONIC COMBUSTION TEST RESULTS**

**4.1 FUEL INJECTION TESTS WITH THE 27.5-DEG RAMP MODEL**

Hydrogen fuel was injected from the row of sonic orifices (normal injection), as in the previous 25-deg ramp model tests. The dimensionless ratio of static to pitot pressure measured at the exit plane of the combustor, along with estimated Mach numbers at the exit plane, is shown in Fig. 13. The measured pressures indicate combustion occurred; however, the dimensionless heat-transfer rates shown in Fig. 14 did not corroborate this. Since combustion causes heat release and hence a pressure increase in a confined channel flow, the heat-transfer rate should increase if significant heat release occurs. In addition, no measurable output was obtained from the radiation sensor gages. A closer look at Fig. 13 shows that the combustion results for normal injection appear to be confined to one side of the model (solid symbol,  $P_{C7} / P'_{O4}$ , see Fig. 3), whereas the heat-transfer rate and radiation sensor gages are on the axial centerline. Thus, it is plausible for these gages to indicate no combustion under these conditions. With no fuel injection, the average static pressure was  $\approx 0.92$  atm, the static temperature was  $\approx 1340^\circ\text{K}$ , and the combustor flow Mach number was  $\approx 1.9$ . These conditions should have been adequate for spontaneous combustion if the injected fuel mixed rapidly with the combustor airflow. It was tentatively concluded that the combination of cold hydrogen ( $300^\circ\text{K}$ )

injection into a boundary layer in proximity to a cold (300°K) combustor wall resulted in a long ignition delay (similar conclusions were obtained for slot injection in Ref. 13), hence a new mode of injection was tested. Diamond airfoil injectors (see Figs. 3 and 4) were installed. The hydrogen was injected from sonic orifices, in the airfoil (strut) surface, which were located several diameters from the cold combustor wall. Combustion could be detected from pressure measurements (denoted by a circular symbol in Fig. 13), heat-transfer rates (Fig. 14), and radiation gage sensor output (Fig. 15).

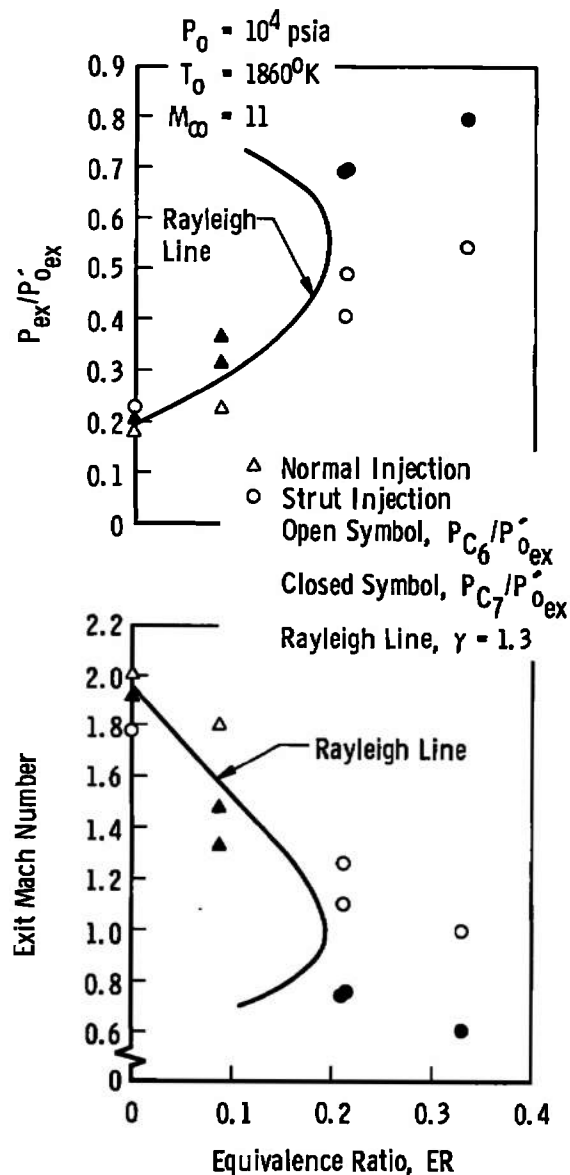


Fig. 13 Dimensionless Combustor Exit Pressures versus Equivalence Ratio (Cold Driver)

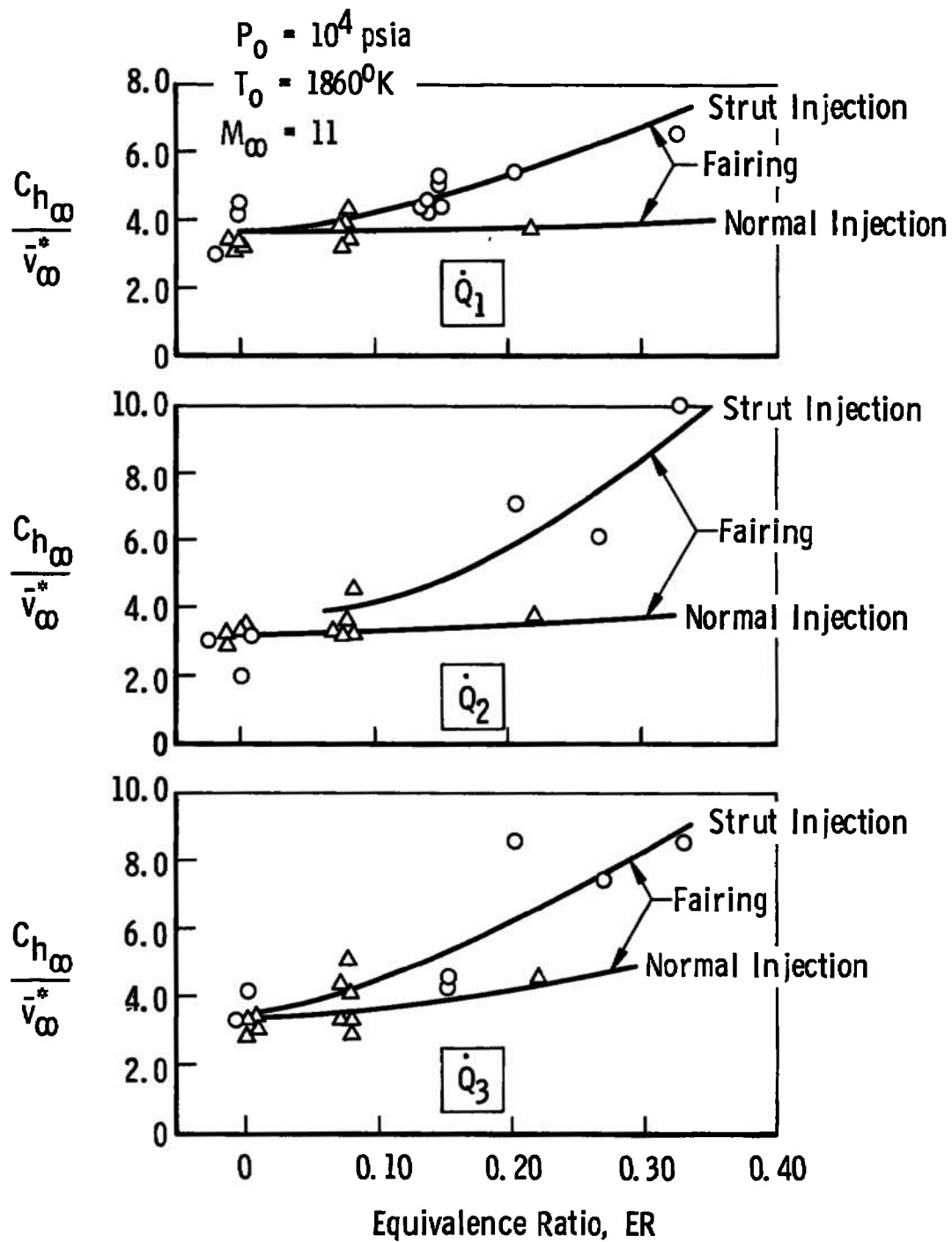


Fig. 14 Dimensionless Combustor Heat-Transfer Rates versus Equivalence Ratio (Cold Driver)

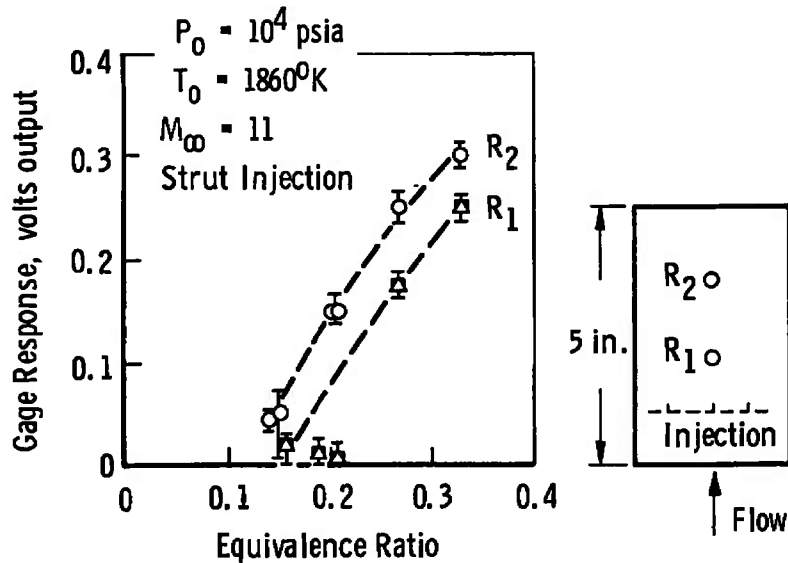
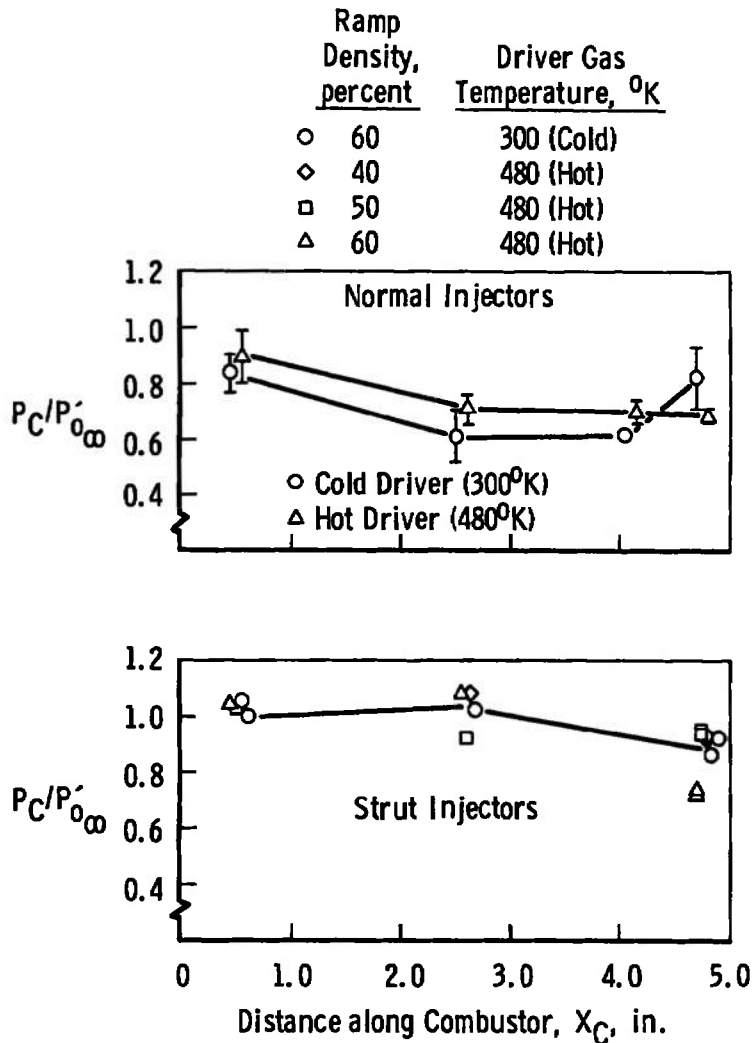


Fig. 15 Relative Output of Radiation Gages versus Equivalence Ratio (Cold Driver)

#### 4.2 27.5-DEG RAMP MODEL TESTS WITH HEATED SHOCK TUNNEL DRIVER GAS OPERATION

The driver gas (helium) was heated to  $\approx 480^{\circ}\text{K}$ , which resulted in an increase in total enthalpy of  $\approx 30$  percent. It was hoped that this increase in enthalpy would improve the static conditions in the combustor sufficiently to obtain combustion data across the whole channel for normal injection. Tests without fuel injection resulted in the dimensionless combustor pressures shown in Fig. 16. The tests were conducted with and without the airfoil struts installed. An increase in pressure level was obtained because of an approximately 10-percent increase in reflected shock pressure (reservoir or total pressure). With a combustor static pressure of  $\approx 1.23$  atm, the estimated static temperature was  $\approx 1530^{\circ}\text{K}$ , and the estimated flow Mach number was  $\approx 1.9$ .

During a series of tests, the 60-percent dense porous ramp became damaged and was replaced by a more porous ramp (50-percent dense). Some improvement in pressure recovery was obtained, as shown in the table in Fig. 16; thus after a number of tests, it was replaced by a 40-percent dense porous ramp. No additional increase was obtained, and since the ramp was quite porous, it rapidly became damaged (by shock tube diaphragm particles); hence no further tests were made with this ramp.



Combustor Exit Pitot Pressure				
Injector Type	Ramp Density, percent	Driver Gas	$P_{03}'/P_{0\infty}'$ ±10 percent	$P_{04}'/P_{0\infty}'$ ±10 percent
Normal	60	Cold	4.70	3.90
Normal	60	Hot	4.40	3.93
Strut	60	Cold	3.85	3.00
	60	Hot	3.65	3.55
	40		4.32	4.20
	50		4.40	4.00

Fig. 16 Effect of Driver Gas Temperature and Ramp Density on Dimensionless Combustor Pressures (27.5-deg Ramp Model)

### 4.3 FUEL INJECTION TESTS WITH THE 27.5-DEG RAMP MODEL AND HEATED DRIVER GAS OPERATION

Combustion testing was resumed with similar results to those obtained with a cold driver, as shown in Fig. 17. Dimensionless heat-transfer rates and radiation sensor gage outputs were similar to the results of Figs. 14 and 15. A summary plot of the axial pressure distribution as a function of equivalence ratio is shown in Fig. 18. An approximate upper limit for equivalence ratio for constant area combustion is 0.2 at a Mach number of 2, and a test with an overall equivalence ratio of 0.3 did, in fact, produce thermally choked flow, as shown in Fig. 18. Exit Mach numbers were estimated from the ratio of exit static to exit pitot pressures.

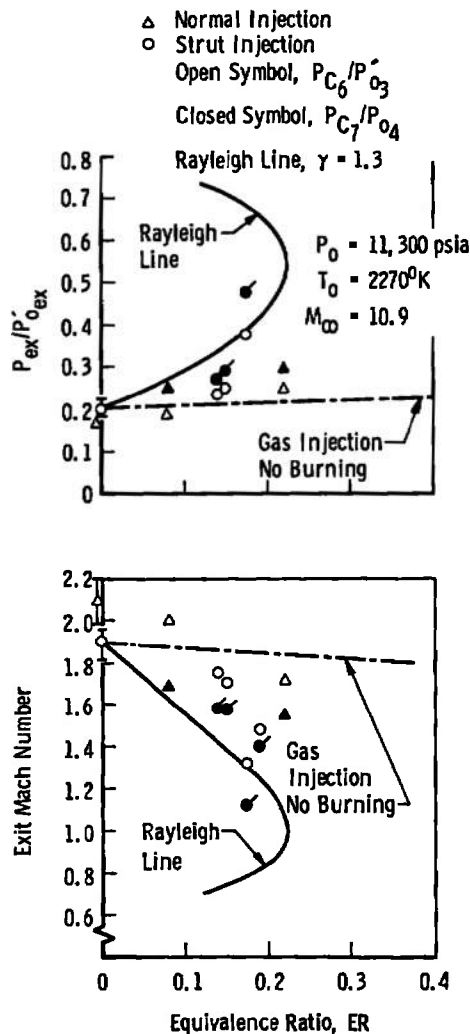


Fig. 17 Dimensionless Combustor Exit Pressures versus Equivalence Ratio (Hot Driver)

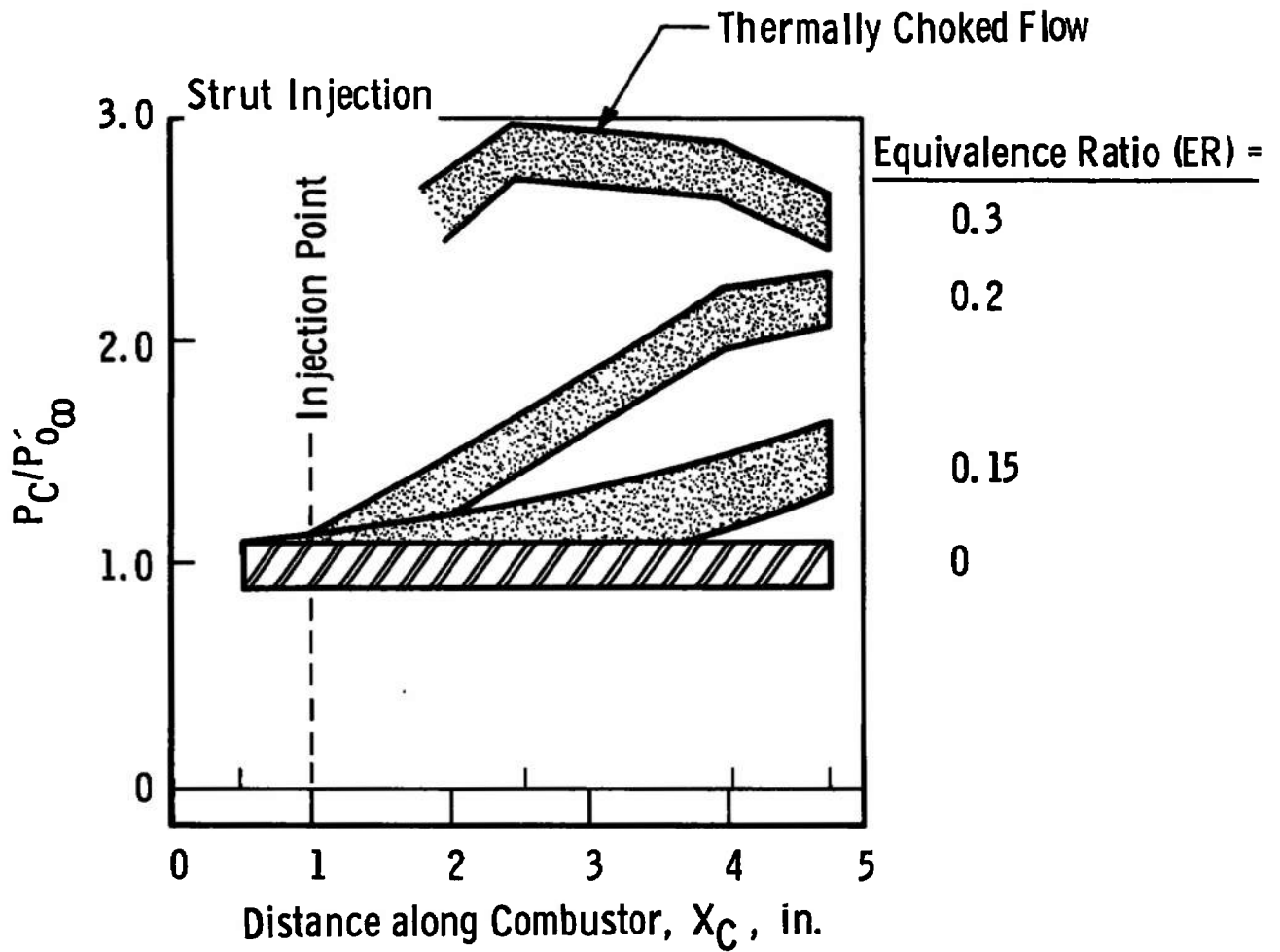


Fig. 18 Influence of Equivalence Ratio on Combustor Static Pressure Distribution

#### 4.4 SODIUM LINE REVERSAL TEMPERATURE MEASUREMENTS

The static temperature in the combustor was measured using the line reversal method described previously. After a number of development tests, static temperatures were obtained for two equivalence ratios, as shown in Fig. 19. During several of these tests, the oscilloscope base line shifted. This shift was attributed to either dirt on the model combustor windows or movement of the knife edge or field stop (see Fig. 8) caused by excessive vibration. If either of these effects were thought to have occurred during the shot, the results were discarded. Additional experience and development with the equipment should improve the data acquisition.

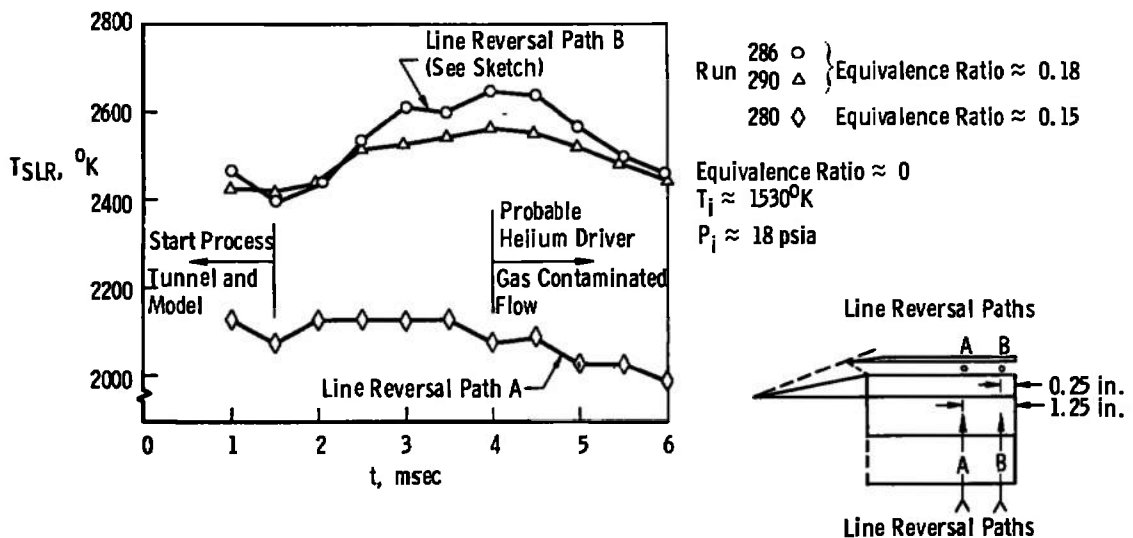


Fig. 19 Line Reversal Temperatures as a Function of Time

The measured temperatures (particularly along path B) were significantly higher than would be expected for constant area combustion, based on an equivalence ratio computed from the ratio of total hydrogen/air mass flow rates, as shown in the theoretical analysis described later. From a physical standpoint, higher temperatures could be expected if the local equivalence ratios were higher than the computed mean value, since line reversal temperature measurements are strongly biased towards the hottest zone through which the light from the comparison source travels. Some nonequilibrium chemical kinetic calculations were carried out in an attempt to define the experimental combustion process. The results of these calculations are discussed in detail in the next section.

## SECTION V THEORETICAL COMBUSTION CALCULATIONS

The mechanism of the experimental mixing and combustion process is considered to be a combination of the following processes:

1. Hydrogen is injected from a number of small diameter, sonic orifices as discrete jets, perpendicular to the strut surface and the combustor airflow, and each jet is turned parallel to the airstream in a distance governed by the local dynamic pressure and shear forces (see Ref. 14).
2. The jets on each side of a strut entrain air, and in so doing the individual jet boundaries expand until they merge with each other and the combustor wall. Further entrainment occurs, and the jet boundary expands laterally, since the walls constrain the upper and lower jet boundaries. At some distance downstream, the jets from different struts will begin to merge until eventually (if the channel is long enough) the hydrogen/air mixture will become approximately uniform.
3. This complicated mixing process becomes more complicated in the experiment since at some small distance downstream of the struts, spontaneous ignition takes place, and the mixing process is affected by heat release caused by chemical reaction. A theoretical model for this process of mixing and reaction would be exceedingly complicated; thus a very simplified model was assumed in which the mixing had already occurred, i. e., the flow was assumed to be premixed. The object of the simplified model was to determine whether the real combustion process could be evaluated from a comparison of the computed and experimental pressures and temperatures. The nonequilibrium chemistry program of Ref. 15 was used to determine the static pressure and temperature distribution along a combustor for a range of equivalence ratios. Results for constant area combustion are shown in Fig. 20, and results for constant pressure combustion are shown in Fig. 21. The values obtained from experiments are plotted as open circles in each figure. Comparison of the experimental and theoretical results indicates that the real process lies

between that for constant area combustion and constant pressure combustion for the following reasons:

- a. The computed temperature for constant area combustion is significantly less than the experimental value for the same equivalence ratio (based on total hydrogen and air mass flow rates).
- b. The computed pressures for constant area combustion are less than the experimental values. (Note, however, the disagreement between combustor exit temperatures.)
- c. The equivalence ratio required to match the computed and experimental temperatures for constant pressure combustion is significantly greater than the mean experimental value.
- d. The maximum value of equivalence ratio for constant area combustion is  $ER < 0.275$  (for the flow conditions described earlier) to prevent thermal choking; however, an ER of 0.25 results in a computed pressure greater than the experimental value.

A more realistic theoretical model is currently being developed which will use the experimental measurements (pressure, heat transfer, and temperature) as control variables. Additional instrumentation techniques are being developed to complement this study.

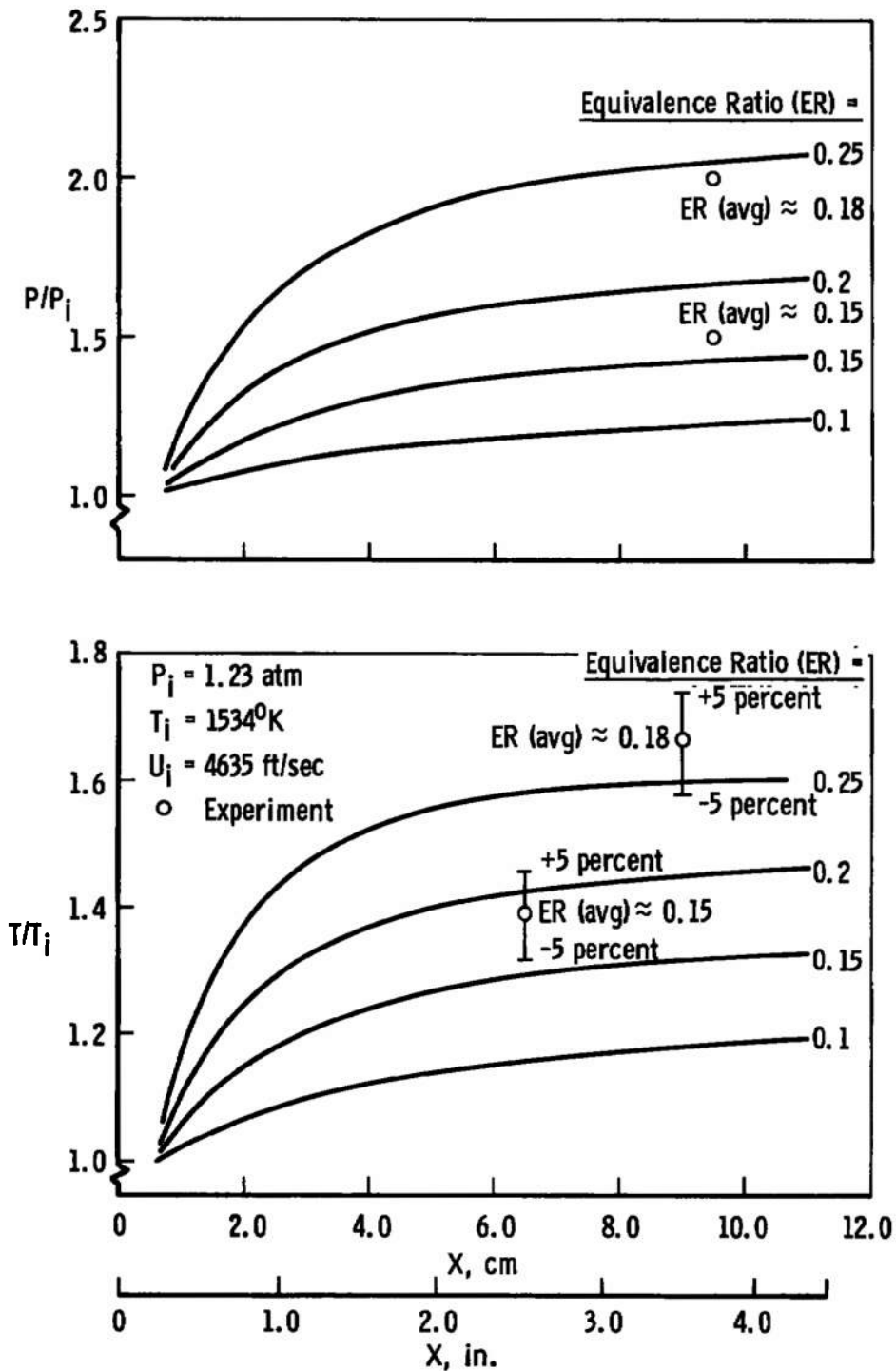


Fig. 20 Effect of Equivalence Ratio on Combustor Static Pressures and Temperatures for Constant Area Combustion (Nonequilibrium Theory)

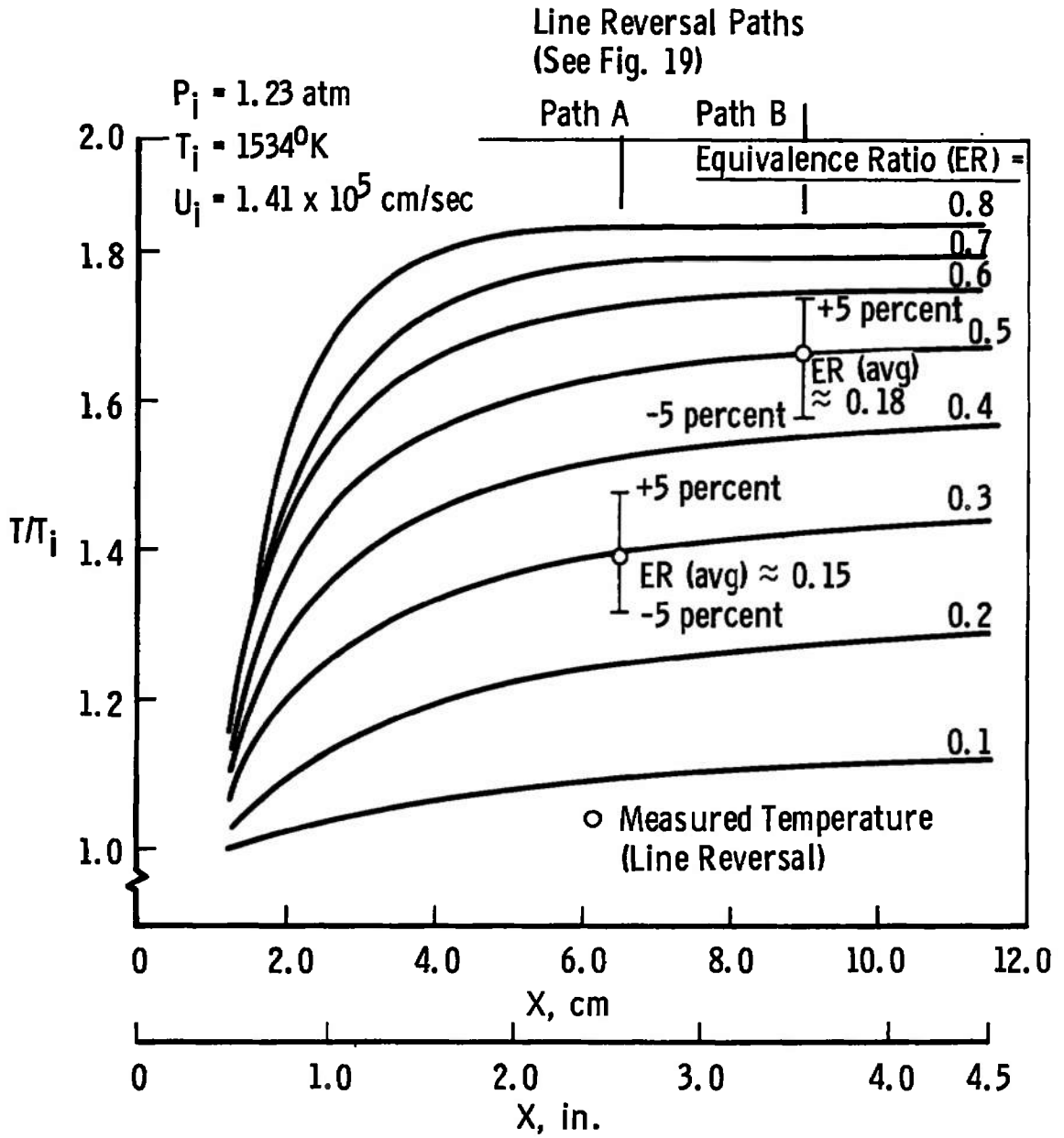


Fig. 21 Effect of Equivalence Ratio on Cambuster Static Temperature for Constant Pressure Combustion (Nonequilibrium Theory)

## SECTION VI CONCLUSIONS

1. A double-oblique-shock scramjet model has been developed with which it is possible to carry out supersonic combustion tests for development of instrumentation and analytical techniques within the useful test time of approximately 3 msec.
2. The boundary layer generated on the inlet was shown to have considerable influence on the total and static pressure recovery through separation effects induced by the shock from the cowl lip and the Prandtl-Meyer expansion at the junction of the inlet and combustor.
3. The highest pressure recovery, coupled with a uniform pressure distribution, was obtained with a porous inlet ramp and a model configuration in which the shock from the cowl lip impinged closest to the junction of the inlet and combustor. This configuration allows the most effective cancellation of the Prandtl-Meyer expansion at the junction.
4. Supersonic combustion in the hot shock tunnel driver tests was verified by the combined measurements in the combustor of static pressures, pitot pressures, surface heat-transfer rates, radiation sensor gages, and line reversal temperatures.
5. Nonequilibrium chemical kinetic calculations were carried out to define the combustion process. It was shown that local values of equivalence ratio in the model combustor were greater than the computed average value and that the combustion process appears to be between combustion at constant area and combustion at constant pressure.

## REFERENCES

1. Ball, H. W. "Calibration of the 100-Inch Hypervelocity Tunnel." AEDC-TDR-63-46 (AD298279), March 1963.

2. Griffith, B. J. and Weddington, E. D. "Recent Refinements and Advancements of Hypersonic Testing Techniques in the 100-Inch Tunnel F of the von Kármán Gas Dynamics Facility." Proceedings of the Fourth Hypervelocity Techniques Symposium, Arnold Engineering Development Center, November 15-16, 1965.
3. Osgerby, I. T. and Smithson, H. K. "Operation of AEDC-VKF 100-in. Hotshot Tunnel F with Air as a Test Gas and Application to Scramjet Testing." AEDC-TR-67-242 (AD664906), December 1967. Also presented at the Fifth Hypervelocity Techniques Symposium, University of Denver, Colorado, March 1967.
4. Rhodes, R. P., Rubins, P. M., and Chriss, D. E. "The Effect of Heat Release on the Flow Parameters in Shock-Induced Combustion." AEDC-TDR-62-78 (AD275366), May 1962.
5. Rubins, P. M. and Rhodes, R. P. "Shock-Induced Combustion with Oblique Shocks, Comparison of Experiment and Kinetic Calculations." AEDC-TDR-63-103 (AD405887), June 1963. Also AIAA Journal, Vol. 1, No. 12, December 1963, pp. 2778-2784.
6. Osgerby, I. T., Smithson, H. K., and Wagner, D. A. "Development of a Double-Oblique-Shock Scramjet Model in a Shock Tunnel." AEDC-TR-69-59, August 1969.
7. Ball, H. W. "Initial Operation of the Pilot Counterflow Test Unit (I)." AEDC-TR-65-132 (AD465893), July 1965.
8. Haun, J. H. and Ball, H. W. "Calibration of the Shock Tunnel Component of Counterflow Range (I) at Mach 7.5." AEDC-TR-66-64 (AD632816), May 1966.
9. Ledford, R. L., Smotherman, W. E., and Kidd, C. T. "Recent Developments in Heat Transfer Rate, Pressure, and Force Measurements for the Hotshot Tunnels." Paper presented at the Second International Congress on Instrumentation in Aerospace Simulation Facilities, Stanford University, August 29-31, 1966.
10. Penner, S. S. Quantitative Molecular Spectroscopy and Gas Emissivities. Addison Wesley Publishing Company, Inc., Reading, Massachusetts, 1959.

11. Nadaud, L. and Giegnel, M. "Mesuré Optiques des Temperatures Elevees." Reprint from AGARDograph 68, High Temperature Aspects of Hypersonic Flow. AGARD-NATO Specialists' Meeting, Belgium, April 3-6, 1962. Also "Optical Measurement of High and Quickly-Variable Temperatures, 'MT4', ONERA Pyrometer." Office National D'etudes et Recherches Aero-spatiales.
12. Pergament, H. S. "Theoretical Analysis of Non-Equilibrium Hydrogen-Air Reactions in Flow Systems." AIAA-ASME Hypersonic Ramjet Conference, April 1963, Paper No. 63-113.
13. Schetz, J. A. and Favin, S. "Analysis of the Ignition of Slot-Injected Gaseous Hydrogen in a Supersonic Air Stream." AIAA Second Propulsion Joint Specialists Conference, Colorado Springs, Colorado, June 1966, Paper No. 66-644.
14. Schetz, J. A. and Billig, F. S. "Penetration of Gaseous Jets Injected into a Supersonic Stream." Journal of Spacecraft and Rockets, Vol. 3, No. 11, November 1966, pp. 1658-1665.
15. Osgerby, I. T. "A Simplified Method for Solving Problems Involving Chemically Reacting One-Dimensional Flows." AEDC-TR-68-268 (AD683260), March 1969.

## DOCUMENT CONTROL DATA - R &amp; D

(Security classification of title, body of abstract and indexing annotation must be entered when the overall report is classified)

1. ORIGINATING ACTIVITY (Corporate author) Arnold Engineering Development Center ARO, Inc., Operating Contractor Arnold Air Force Station, Tennessee 37389		2a. REPORT SECURITY CLASSIFICATION UNCLASSIFIED	
		2b. GROUP N/A	
3. REPORT TITLE SUPERSONIC COMBUSTION TESTS WITH A DOUBLE-OBLIQUE-SHOCK SCRAMJET IN A SHOCK TUNNEL			
4. DESCRIPTIVE NOTES (Type of report and inclusive dates) June 1967 through December 1968 - Final Report			
5. AUTHOR(S) (First name, middle initial, last name) I. T. Osgerby, H. K. Smithson, and D. A. Wagner, ARO, Inc.			
6. REPORT DATE February 1970		7a. TOTAL NO. OF PAGES 38	7b. NO. OF REFS 15
8a. CONTRACT OR GRANT NO. F40600-69-C-0001		9a. ORIGINATOR'S REPORT NUMBER(S) AEDC-TR-69-162	
b. PROJECT NO. 3012		9b. OTHER REPORT NO(S) (Any other numbers that may be assigned this report) N/A	
c. Program Element 62402F			
d. Task 07			
10. DISTRIBUTION STATEMENT This document has been approved for public release and sale; its distribution is unlimited.			
11. SUPPLEMENTARY NOTES Available in DDC.		12. SPONSORING MILITARY ACTIVITY Arnold Engineering Development Center, Air Force Systems Command, Arnold Air Force Station, Tenn. 37389	
13. ABSTRACT Some results of a continuing research program to develop a capability for testing integrated scramjets in the AEDC Tunnel F (Hotshot) are reported here. During this research program, an integrated double-oblique-shock scramjet model was developed to provide a test bed for supersonic combustion tests and for instrumentation development essential for analysis of combustion test results. Results are presented for tests in which hydrogen fuel was injected into the combustor. Injection of the fuel, from sonic orifices in the wall, normal to the flow did not lead to satisfactory combustion data, supposedly because of the cold boundary layer. Injection through sonic orifices in a series of diamond airfoil injectors led to combustion confirmed by all the following measurements (1) an increase in static pressure within the combustor downstream of the injection station, (2) an increase in surface heat-transfer rate, (3) an increase in static temperature as measured by the sodium line reversal technique, (4) an increase in output of radiation sensor gages, and (5) a decrease in flow Mach number inferred from static to pitot pressure measurements. The measured increases were proportionate to increases in computed average equivalence ratio. The combustion results are compared with numerical solutions. In general, the measured temperatures and pressures in the combustor with heat addition were higher than the calculated values.			

